JOURNAL OF NANO- AND ELECTRONIC PHYSICS
Vol. 11 No 4, 04008(6pp) (2019)
ЖУРНАЛ НАНО- ТА ЕЛЕКТРОННОЇ ФІЗИКИ
Том 11 № 4, 04008(6cc) (2019)

Simulation of Guard Ring Type Effects on the Electrical Characteristics of *n*-on-*p* Planar Silicon Detectors

M. Mekheldi[1,2,*], S. Oussalah[2,†], A. Lounis[3], N. Brihi[1]

[1] *Université Mohammed Seddik Benyahia de Jijel, Ouled Aissa, 18000 Jijel, Algeria*
[2] *Centre de Développement des Technologies Avancées, Cité 20 août 1956, Baba Hassen, 16303 Algiers, Algeria*
[3] *Laboratoire de l'Accélérateur Linéaire, Université Paris-Sud XI, CNRS/IN2P3, Orsay, France*

(Received 20 December 2018; revised manuscript received 26 June 2019; published online 22 August 2019)

The upgrades of high-energy physics experiments at the Large Hadron Collider (LHC) at CERN will call for new radiation hard technologies to be applied in the next generations of tracking devices that will be required to withstand extremely high radiation doses. *N*-on-*p* planar pixel sensors are promising candidates and to be implemented in the future ATLAS pixel detector. In this work, we present a comparative study for two different designs of multi-guard structures, before and after irradiation. Both structures are based on the *p*-type substrate technology with and without p-stop isolation between implants. Moreover, one structure has *p*-type guard rings while the other has n-type ones. Various technological parameters are varied like thickness and doping of the silicon substrate, depth and doping of the guard rings, and thickness of the silicon dioxide to study the electrical performances of the structures. The performance of the multi-guard ring structures are evaluated with TCAD simulations up to a radiation fluence of 1×10^{16} n_{eq}/cm^2 using an existing p-type bulk radiation damage model based on the so called "Perugia three level traps model", where irradiation generates two acceptor levels, positioned slightly above the mid bandgap, and one donor level, located below the mid bandgap. We have considered an increasing amount of oxide charge with the irradiation dose. For a good quality SiO_2 layer, an initial charge density at the interface layer was set to 5×10^{10} cm^{-2} for a non-irradiated detector, whereas for a heavily irradiated structure the charge density value can reach 1×10^{12} cm^{-2}. They have been simulated on high resistivity silicon wafers using Silvaco Virtual Wafer Fab (VWF) software.

Keywords: Breakdown voltage, Guard rings, Planar silicon detector, Radiation damage, TCAD simulation.

DOI: 10.21272/jnep.11(4).04008 PACS numbers: 07.05.Tp, 85.30.Mn, 29.40. – n

1. INTRODUCTION

Pixelated silicon detectors are the most precise devices for charged particle tracking currently in use at high-energy physics (HEPs) in ATLAS (A Toroidal LHC ApparatuS) experiment at CERN (European Organization for Nuclear Research), Geneva. Located close to the interaction point, the silicon detectors are required to function in a radiation harsh environment [1-3], Furthermore, they are required to be operated at a high voltage to maximize the signal and reduce the charge collection time.

In almost all experiments, at Large Hadron Collider (LHC) multi-guard ring structures are used for silicon strips and pixel detectors. This system can offer a solution if the optimization of the design takes into account the radiation effects. The multi-guard ring structure is a set of electrodes with associated implants surrounding the active area of the sensor. The aim of this structure is to control the potential drop from electrodes in the active area of the sensor to the cutting edge of the device. The guard rings are biased by a punch-trough mechanism creating a current circulating between the guard rings [2]. The distance between guard rings and the metal overlap have a great impact on the potential drop [4].

P-type bulk silicon detectors are expected to be more radiation hard than standard *n*-type one [5-8]. However, the *n*-on-*p* conception requires inter pixel insulation that is why they considered complex. This insulation between pixels in order to compensate the electron layer formed below the oxide that would short out the n^+ implantations. There are two commonly used ways to prevent this. In each case, a *p*-layer insulates the n^+ pixels. The insulation is achieved by a blank surface implant named p-spray or by *p*-type junctions named p-stops. In the p-spray option, the whole surface is lightly doped [9]. In the *p*-stop version, separate heavily doped junctions are used. Till now, there is no guard ring structure for the n-on-p technology has been established [10-12]. Koybasi et al. [13] have proposed a new design of the guard ring structure for *n*-on-*p* sensors for different application domains taking example high luminosity research field as feature of the proposed form, the non-existing of isolation between the guard rings implants.

The contribution in this work is to make a comparative study between the electrical performances of both structures of sensors *n*-on-*p* with p-type guard rings [13] and *n*-on-*p* with *n*-type guard rings using TCAD simulation tools. The influence of different structure parameters such as, substrate thickness, substrate doping, guard ring depth, and oxide thickness on the electrical characteristics was investigated. The main focus of the device simulations is to develop an approach to model and predict the performance of the irradiated silicon detectors using professional software, namely Silvaco Atlas [14].

* mmekheldi@cdta.dz
† soussalah@cdta.dz

 © 2019 Sumy State University

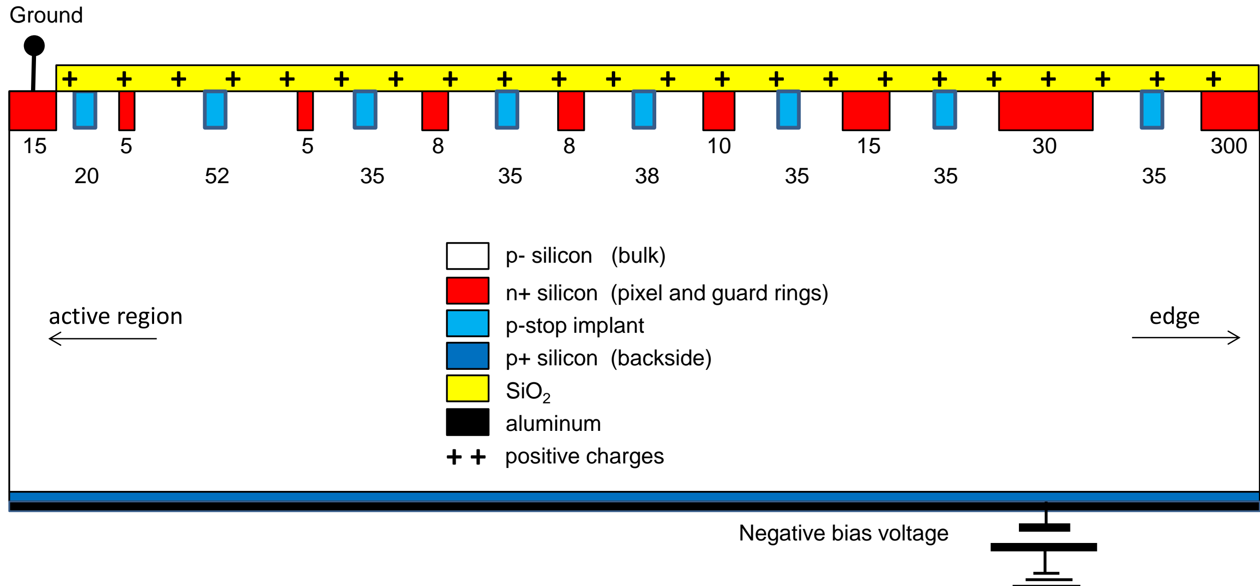

Fig. 1 – The sketch drawing of n-on-p sensor technology with n-type guard rings isolated by p-stop implants. All dimensions are in μm

The rest of this paper is organized as follows. Section 2 is reserved to describe two different *n*-on-*p* silicon detector structures studied in this paper. In section 3, we present the obtained TCAD simulation results for both structures with a comparative study between them. Finally, in section 4, some remarks and conclusions are provided with future works.

2. STRUCTURES AND TCAD SIMULATION

2.1 Structures

The *n*-on-*p* silicon detector structures simulated in this study are: the first one is *p*-type guard rings proposed by Koybasi et al. [13] and the second one is n-type guard rings shown in Fig. 1. In the following, the first structure is named "*p*-GR" and the second one is named "*n*-GR". For both structures, the bulk material is low p-type silicon doping. Eight guard rings with different width and spacing between them surround the *n*-type pixel. High voltage electrode doping is *p*-type.

2.2 TCAD Simulation

The Technology Computer-Aided Design (TCAD) simulations have been performed with Atlas Silvaco software [14]. Atlas simulator provides general capabilities for physically-based two and three-dimensional simulation of semiconductor devices. Atlas enables the electrical, optical, and thermal characterization and optimization of semiconductor devices for different types of technologies under different conditions.

The simulation program containing different steps starting by mesh defining are discrete elements as an input structure followed by the determination of regions and materials. The AC, DC, and transient electrical characteristics are obtained by solving the Poisson's, continuity and mobility equations at every grid node.

More parameters can be obtained and visualized with Tonyplot module such as carrier mobility and potential distribution inside the semiconductor.

Bipolar is a material model specification employed in the simulation that contains different physical models such as CONMOB (concentration dependent mobility), FLDMOB (field dependent mobility), CONSRH (Schokley-Read-Hall recombination using concentration dependent lifetimes), AUGER (recombination accounting for high-level injection effects), and BGN (band gap narrowing) [14]. Impact ionization is an important phenomenon to be taken into account in the design of various semiconductor devices. As impact ionization is both electric field and temperature dependent, it is crucial to use a model that has the correct functional behavior. In Atlas, the Selberherr's model [15] is used among other models to predict the impact ionization effect in semiconductor devices, which is the generation of free carriers (electrons, holes) mechanism resulting the avalanche breakdown.

In our simulation, the refined mesh was located at the p-n junction and the interface between silicon and silicon dioxide with a maximum height of 0.2 and width of 0.5 μm to ameliorate the accuracy of the obtained results. Simulation software users must carefully allocate mesh nodes at the defined regions as well as define fine meshes at regions of high activity.

3. SIMULATION RESULTS

3.1 No Bulk Radiation Damage and No Oxide Charge

At the beginning, we simulate current-voltage characteristics for the two structures with no bulk radiation damage and no oxide charges. The structures are reverse biased for breakdown voltage simulation. In Fig. 2, the current-voltage characteristics are shown. The simulations were carried out with a substrate thickness of 300 μm and substrate doping of 5×10^{11} cm^{-3}. The pixel and the guard rings depth are of 1.5 μm and the implants doping are about 1×10^{18} cm^{-3}. The doping of p-stop implant and high voltage electrode are 1×10^{17} cm^{-3} and 1×10^{19} cm^{-3}, respectively.

Fig. 2 shows that there is a continuous thermal generation of electron-hole pairs in the depletion region. This is the leakage current (or dark current) seen. As the bias increases, the depletion region grows and the leakage current grows. Once the whole substrate wafer is depleted, the leakage current will remain constant. The characteristics in Fig. 3 show obvious knee points where the reverse current turns to increase dramatically with voltage. The breakdown voltage is easily extracted from the current-voltage characteristics by recognizing the knee point. One can see that the leakage current of the *n*-GR structure is a little bit greater than that of the *p*-GR structure. On the other hand, the breakdown voltage of the *n*-GR structure is much lower than that of the *p*-GR structure. The difference is about 200 V.

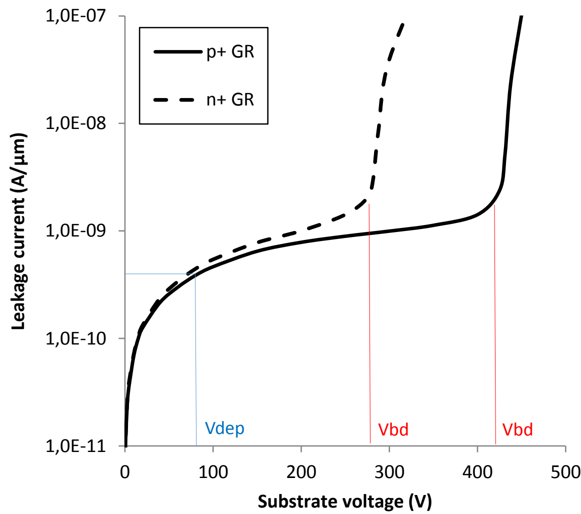

Fig. 2 – Current-voltage characteristics for both structures with no bulk radiation damage and no oxide charges. V_{dep} and V_{bd} are mean depletion voltage and breakdown voltage, respectively

3.2 No Bulk Radiation Damage with Oxide Charge

3.1.1 Oxide Parameters Effect

The present positive charge in the SiO_2 increases with radiation and consequently creates a thin conductive layer at Si/SiO_2 interface. Fig. 3 shows that for both structures breakdown voltage increases with oxide charge until a maximum value and then decreases. The maximum value for the *p*-GR structure is about 6×10^{11} cm^{-2} while for the *n*-GR structure is 4×10^{11} cm^{-2}. On the other hand, a value of 4×10^{11} cm^{-2} was found in [13] for the p-GR structure obtained with Synopsys Sentaurus TCAD. We note that the results obtained with the standard parameters of Synopsys Sentaurus simulation software are definitely different from the results with the standard parameter set of Silvaco Atlas TCAD [16-18]. The decrease in breakdown voltage at a given oxide charges lower than the optimum oxide charge value is due to the non-uniform distribution of potential along the guard rings while at oxide charge higher than the last value it is mainly due to more abrupt potential drop at each guard ring [13].

It can be seen from the results of Fig. 4 that there is no influence of oxide thickness variation on both *p*-GR and *n*-GR structures. Nevertheless, one can see that the breakdown voltage values of the *p*-GR structure remain higher compared to those *n*-GR structure.

3.1.2 Substrate Parameters Effect

Thin silicon substrate is one of the possible choices to reduce material budget in high-energy experiments. Thinner substrate reduces carrier multiple scattering in the detector and therefore diminishes the carrier trapping probability in the bulk and as a result the charge collection efficiency is improved [19, 20]. As shown in Table 1, the doping concentration is kept at a constant value of 5×10^{11} cm^{-3}. As the substrate thickness increases from 150 µm to 300 µm the breakdown voltage increases too for both structures. The decrease of the breakdown voltage is more significant for the *p*-GR structure than the *n*-GR. However, the higher the substrate thickness, the better the electrical performance. In Table 2, the thickness of substrate is 300 µm. It is shown that higher breakdown voltage is due to lower doping substrate. On the other hand, the leakage current is not influenced by the variation of the thickness and doping of the substrate for both structures.

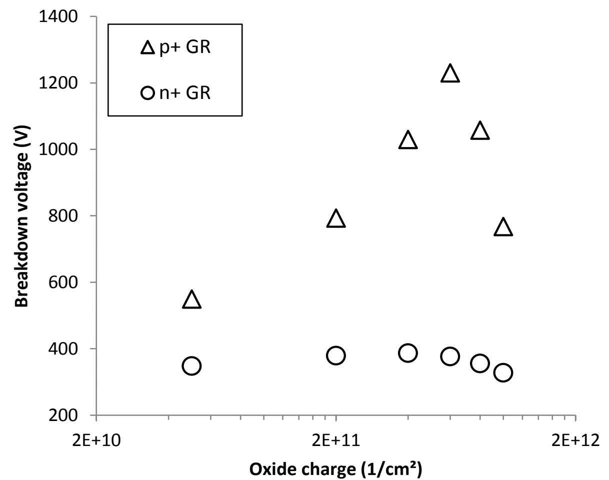

Fig. 3 – Breakdown voltage as a function of oxide charges for both structures

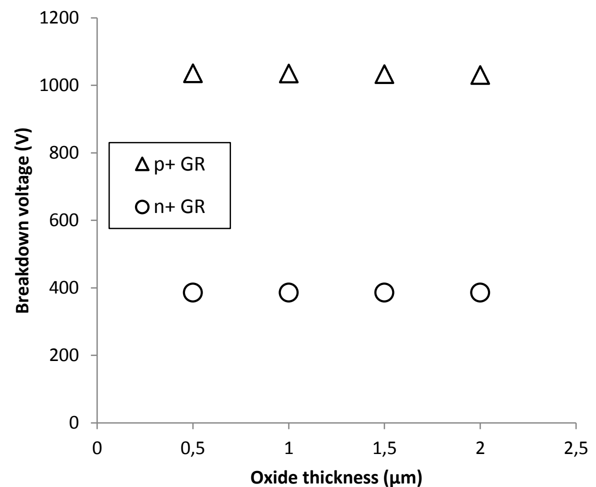

Fig. 4 – Breakdown voltage as a function of oxide thickness for both structures

Table 1 – Breakdown voltage as a function of substrate doping for both structures

	Breakdown voltage (V)	
Substrate thickness (μm)	p^+ GR	n^+ GR
150	790	342
200	897	361
250	976	376
300	1036	386

Table 2 – Breakdown voltage as a function of substrate ring thicknes for both structures

	Breakdown voltage (V)	
Substrate doping (cm^{-3})	p^+ GR	n^+ GR
$1\times10^{+11}$	1060	404
$5\times10^{+11}$	1036	386
$1\times10^{+12}$	1007	365
$5\times10^{+11}$	804	276

Table 3 – Breakdown voltage as a function of guard ring depth for both structures

	Breakdown voltage (V)	
Guard ring depth (μm)	p^+ GR	n^+ GR
0.5	1187	377
1	1103	383
1.5	1035	386
2	973	395
2.5	920	459

Table 4 – Breakdown voltage as a function of guard ring doping for both structures

	Breakdown voltage (V)	
Guard ring doping (cm^{-3})	p^+ GR	n^+ GR
$1\times10^{+17}$	1042	385
$1\times10^{+18}$	1035	385
$1\times10^{+19}$	1036	386

3.1.3 Guard Ring Parameters Effect

Guard ring doping profile parameters effect has been considered. First, the guard ring doping concentration value is fixed at 10^{18} cm^{-3} and the guard ring profile depth is varied from 0.5 to 2.5 μm. Second, the depth of the guard ring profile is kept at 1.5 μm and the doping is varied from 10^{17} to 10^{19} cm^{-3}. As shown in Table 3, when the depth of the guard ring profile increases the breakdown voltage of the p-GR structure decreases significantly while the breakdown voltage of the n-GR structure increases smoothly. Therefore, we conclude that the p-type guard ring depth must be as shallow as possible for the p-GR structure. Table 4 shows that there is no influence of the doping concentration on the breakdown characteristics for both structures.

3.3 With Bulk Radiation Damage

The principle source of radiation damage in silicon sensors is from non-ionizing-energy-loss (NIEL). It is normally expressed in terms of 1 MeV neutron equivalent for silicon (1 MeV n_{eq}/cm^2). The incident radiation creates defects in the silicon lattice, forming extra energy levels in the band gap of silicon that act as generation-recombination and charge trapping centers. The primary effects of this radiation bulk damage are:

1. a conversion of material from n- to p-type that leads an increase of the bias voltage;
2. an increase in leakage current proportional to the radiation fluence that can lead to local heating and therefore to thermal run away;
3. an increase in depletion voltage due to increasing effective doping concentration;
4. a reduction of the charge collection efficiency (CCE) due to increasing number of traps.

A trap model has been proposed by the University of Perugia [21] to describe radiation damage caused by proton irradiation in p-type FZ silicon. According to the model, the radiation generates two acceptor levels positioned slightly above the mid band gap and one donor level located far below the mid band gap. The details of the trap model are presented in Table 5.

Table 5 – The University of Perugia Trap Model [21]

Defect	$\boldsymbol{E}$ **(eV)**	$\boldsymbol{\sigma_e}$ **(cm^{-2})**	$\boldsymbol{\sigma_n}$ **(cm^{-2})**	$\boldsymbol{\eta}$
Acceptor	$Ec - 0.42$	1.00×10^{-15}	1.00×10^{-14}	1.613
Acceptor	$Ec - 0.46$	7.00×10^{-15}	7.00×10^{-14}	0.9
Donor	$Ev + 0.36$	3.23×10^{-13}	3.23×10^{-14}	0.9

Since the acceptor states are close to the mid bandgap, they will generate electron-hole pairs, increasing the leakage current. A small portion of the acceptor states will be occupied and therefore negatively charged, increasing the effective p-type doping while the unoccupied acceptor states will trap excess electrons in the conduction band. The function of the donor state, which is far below the mid band gap, is to trap excess holes from the valence band.

The post irradiation performance of the guard ring structures has been evaluated with simulations using the trap model presented in Table 5. The simulation has been performed for fluences from 2×10^{14} n_{eq}/cm^2 to 1×10^{16} n_{eq}/cm^2 and for charge oxide from 5×10^{10} cm^{-2} to 1×10^{12} cm^{-2}. For more clarity, only extreme values for each parameter are presented. Fig. 6 shows the breakdown behavior of the guard ring structures after irradiation for two different values of fluence where the oxide charge is fixed at 1×10^{12} cm^{-2}. Fig. 7 shows the breakdown behavior of the guard ring structures after radiation of 1×10^{15} n$_{eq}$/cm^2 for two different values of oxide charge. As one can see, the breakdown behavior degrades significantly with irradiation.

For an oxide charge of 1×10^{12} cm^{-2}, the p-GR structure is able to survive only up to reverse bias of 200 V at fluence of 1×10^{16} n_{eq}/cm^2, while the n-GR structure is able to survive only up to reverse bias of 100 V at the same fluence.

The decrease in breakdown voltage after irradiation is attributed to [13]:

1. the increase of surface conductivity as a consequence of increasing oxide charge, so the potential drop at each guard ring becomes steeper, resulting in higher electric fields;

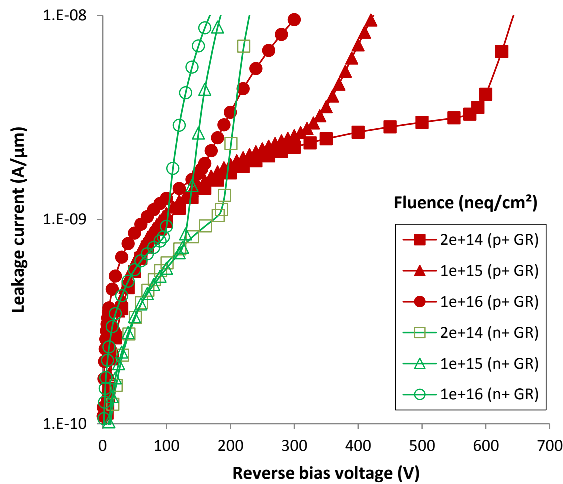

Fig. 6 – Leakage current versus reverse bias voltage at different fluences. The oxide charge is 1×10^{12} cm^{-2}

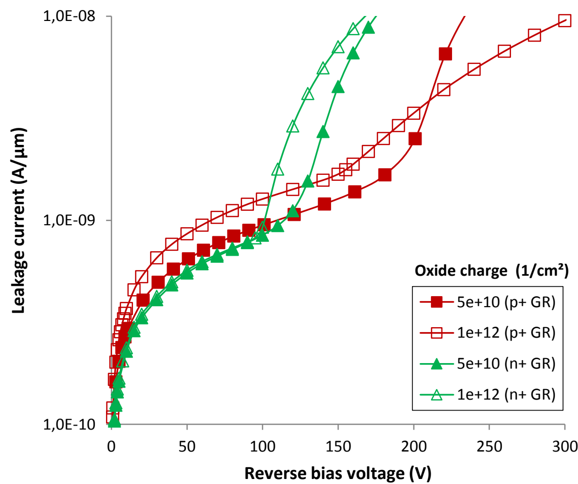

Fig. 7 – Leakage current versus reverse bias voltage for different values of oxide charge after radiation of 1×10^{15} n_{eq}/cm^2

2. the increase of the depletion voltage due to the radiation-induced bulk traps, therefore for a given applied bias voltage, the space charge region volume decreases with irradiation and all potential drops at the guard rings near the pixel since the depletion region does not reach the outer ones.

At a fluence of 1×10^{16} n_{eq}/cm^2 the breakdown voltage for both structures is almost the same but the leakage current of the *n*-GR structure is much lower than the p-GR one when charge saturation takes place. The breakdown voltages for both structures are not high enough for very high luminosity applications, so further improvements are needed.

4. CONCLUSIONS

We have used Silvaco Atlas TCAD device simulator to evaluate the electrical performances of two different high-voltage silicon detectors based on n-on-p technology dedicated to be used in high-energy physics experiments. When the substrate thickness decreases from 300 to 150 the breakdown voltage decreases by 25 % and 11 % for the structures with p-type guard rings and n-type guard rings, respectively. When guard ring depth increases, breakdown voltage decreases for structure with p-type guard rings and increases for *n*-type one. For both structures breakdown voltage increases with oxide charge until a maximum value and then decreases. Oxide thickness has no influence on the breakdown voltage. Without any radiation damage and for an oxide of 4×10^{11} cm^{-2}, the structure featuring *p*-type guard rings can withstand reverse bias voltages above 1200 V while the structure featuring n-type guard rings can withstand only voltages about 400 V. These results demonstrate the superiority of structure with *p*-type guard rings over structure with *n*-type guard rings with *p*-stop isolation technique. Despite these results, at the very high luminosity applications structure with *n*-type guard rings shows better behavior than structure with *p*-type guard rings structure in term of leakage current when oxide charge saturation takes place. An increase in the fluence from 2×10^{14} n_{eq}/cm^2 to 1×10^{16} n_{eq}/cm^2 will decrease the breakdown voltage by approximately a factor of six and two for the structures with p-type guard rings and n-type guard rings, respectively. Our future work will address the optimization of guard rings for high fluences.

AKNOWLEDGEMENTS

The authors would like to thank David Green from Silvaco, Inc. for his support on TCAD simulation, and Dr Walid Filali for his advices and comments.

REFERENCES

1. G. Lindstroem, M. Moll, E. Fretwurst, *Nucl. Instrum. Meth. A* **426** No 1, 1 (1998).
2. G. Lutz, *Semiconductor Radiation Detectors: Device Physics* (Berlin: Springer-Verlag: 2007).
3. D. Djamai, E. Leonidas Gkougkousis, M. Chahdi, A. Lounis, S. Oussalah, *IEEE 41st International Semiconductor Conference (CAS-2018)*, 227 (Sinaia: 2018).
4. F. Hadj Larbi, S. Oussalah, N. Belkhelfa, A. Lounis, *IEEE 26th International Conference on Microelectronics (ICM-2014)*, 14 (Doha: 2014).
5. G. Casse, P. Allport, A. Greenall, *Nucl. Instrum. Meth. A* **581** No1-2, 318 (2007).
6. T. Peltola, *Nucl. Instrum. Meth. A* **796** No1 74 (2015).
7. G. Casse, P. P. Allport, P. R. Turner, S. Marti Garcia, M. Lozano, *Nucl. Instrum. Meth. A* **535** No1-2, 362 (2004).
8. M. Benoit, A. Lounis, N. Dinu, *IEEE T. Nucl. Sci.* **56** No6, 3236 (2009).
9. R.H. Richter, L. Andricek, T. Gebhart, D. Hauff, J. Kemmer, G.Lutz, R. Weiß, A. Rolf, *Nucl. Instrum. Meth. A* **377** No2-3, 412 (1996).
10. Y. Unno, A. Affolder, P. Allport, R. Bates, C. Betancourt, J. Bohm, H. Brown, C. Buttar, J. Carter, G. Casse, *Nucl. Instrum. Meth. A* **636** No1, s24 (2011).
11. L. Evensen, A. Hanneborg, B. S. Avset, M. Nese, *Nucl. Instrum. Meth. A* **337** No1, 44 (1993).
12. N. Bacchetta, G.-F. Della Betta, M. Da Rold, R. Dell'Orso, P.G. Fuochi, A. Lanza, A. Messineo, O. Militaru, A. Paccagnella, G. Verzellesi, R. Wheadon, *IEEE Nuclear Science Symposium Conference Record (NSSMIC-1997), 498 (Albuquerque: 1997)*.
13. O. Koybasi, G. Bolla, D. Bortoletto, *IEEE T. Nucl. Sci.* **57** No5, 2978 (2010).

14. Silvaco Inc., *ATLAS User's Manual Device Simulation Software* (Santa Clara: 2010).
15. S. Selberherr, *Analysis and Simulation of Semiconductor Devices* (New York: Springer-Verlag: 1984).
16. M. Mekheldi, S. Oussalah, A. Lounis, N. Brihi, *Res. Phys.* **6**, 80 (2016).
17. G. Kramberger, *The International Workshop on Vertex Detectors (VERTEX 2016), 1 (Isola d'Elba: 2016).*
18. J. Beyera, M. Bomben, A. Macchioloa, R. Nisiusa, *The 31st RD50 Workshop on Radiation hard semiconductor devices for very high luminosity colliders (RD50 CERN 2017), 1 (Zurich: 2017).*
19. T. Dubbs, S. Kashigin, M. Kratzer, W. Kroeger, T. Pulliam, H.-W. Sadrozinski, M. Schwab, E. Spencer, R. Wichmann, M. Wilder, *Nucl. Instr. Meth. A* **383** No1, 174 (1996).
20. L. Meng, *Development of CMOS sensors for high-luminosity ATLAS detectors, PhD Thesis,* (University of Liverpool: 2018).
21. M. Petasecca, F. Moscatelli, D. Passeri, G. U. Pignatel, *IEEE T. Nucl. Sci.* **53** No5, 2971 (2006).

Моделювання впливу типу захисного кільця на електричні характеристики планарних кремнієвих детекторів типу *n*-on-*p*

M. Mekheldi[1,2], S. Oussalah[2], A. Lounis[3], N. Brihi[1]

[1] *Université Mohammed Seddik Benyahia de Jijel, Ouled Aissa, 18000 Jijel, Algeria*

[2] *Centre de Développement des Technologies Avancées, Cité 20 août 1956, Baba Hassen, 16303 Algiers, Algeria*

[3] *Laboratoire de l'Accélérateur Linéaire, Université Paris-Sud XI, CNRS/IN2P3, Orsay, France*

Оновлення високоенергетичних фізичних експериментів на великому адронному коллайдері (LHC) у ЦЕРНі вимагатиме застосування нових випромінювальних технологій у наступних поколіннях пристроїв стеження, які будуть необхідні для витримування надзвичайно високих доз опромінення. Планарні піксельні датчики *n*-on-*p* є перспективними кандидатами і повинні бути реалізовані у майбутньому піксельному детекторі ATLAS. У роботі представлено порівняльне дослідження двох різних конструкцій багатозахисних структур до і після опромінення. Обидві структури засновані на технології підкладки *p*-типу з та без стопорної ізоляції між імплантами. Більш того, одна структура має захисні кільця *p*-типу, в той час як інша – *n*-типу. Для вивчення електричних характеристик конструкцій змінювалися різні технологічні параметри, такі як товщина і легування кремнієвої підкладки, глибина і легування захисних кілець, та товщина діоксиду кремнію. Ефективність багатозахисних кільцевих структур оцінюється за допомогою моделювання TCAD до флюенсу випромінювання $1\times10^{+16}$ n_{eq}/см^2 з використанням існуючої моделі об'ємного радіаційного пошкодження *p*-типу на основі так званої "Perugia tri level traps model", де опромінення генерує два акцепторних рівня, розташованих трохи вище середньої забороненої зони, і один донорний рівень, розташований трохи нижче середини забороненої зони. Ми розглянули збільшення кількості оксидного заряду з ростом дози опромінення. Для високоякісного шару SiO_2 початкова щільність заряду на інтерфейсному шарі встановлювалася рівною $5\times10^{+10}$ cm^{-2} для неопроміненого детектора, тоді як для сильно опроміненої структури значення щільності заряду може сягати $1\times10^{+12}$ cm^{-2}. Вони моделювалися на високоомних кремнієвих пластинах з використанням програмного забезпечення Silvaco Virtual Wafer Fab (VWF).

Ключові слова: Напруга пробою, Захисні кільця, Планарний кремнієвий детектор, Радіаційні пошкодження, Моделювання TCAD.